

Comparative accuracy study of LDV profile-sensor acquisition modes and particle diameters

Saskia Pasch^{1,*}, Robin Leister¹, Marius Egner¹, Lars Büttner², Jürgen Czarske², Jochen Kriegseis¹

1: Institute of Fluids Mechanics, Karlsruhe Institute of Technology, Germany

2: Laboratory for Measurement and Sensor System Techniques, Faculty of Electrical and Computer Engineering, TU Dresden, Germany

*Corresponding author: saskia.pasch@kit.edu

Keywords: LDV profile sensor, dynamic velocity range, position-estimation uncertainty.

ABSTRACT

The laser Doppler velocity profile sensor (LDV-PS) system offers the possibility to measure flow velocities with high spatial resolution and is therefore a promising method for the investigation of flows with high velocity gradients. The present experimental study revolves around the interplay between a broad range of chosen LDV-PS acquisition parameters, the dynamic velocity range within the observed measurement volume, and the accuracy of the velocity and position estimation from an application perspective. In the chosen set-up, thin wires of different diameters rotate at varying velocity levels and are captured instead of tracer particles by the applied system. It is observed that constant sample rate and number for the Fast Fourier Transform (FFT) evaluation of the detected burst signal allow straightforward measurements of unknown velocity profiles, but imply a velocity-dependent spatial measurement uncertainty. In contrast, velocity-adjusted acquisition settings allow to acquire particle bursts with equal signal resolution and length effecting a constant measurement accuracy at all velocity levels when adjusted appropriately. The position standard deviation is furthermore observed to increase with the wire diameter. Hence, the size of the scattering object should be chosen appropriately small during calibration and measurement. The gained knowledge offers the possibility to adapt the evaluation parameters more specifically to a given measurement problem. Consequently, measurements can be conducted in flows with small velocities with a high spacial resolution, when the FFT parameters and processing routines are adjusted accordingly, small particles are chosen and vibrations in the set-up are avoided.

1. Introduction

Flow velocity measurements with sub-millimeter resolution are of great interest for the experimental investigation of shear flows with strong velocity gradients, such as boundary layers, for instance. Facing this challenging task, a laser Doppler velocity profile sensor (LDV-PS) based on two convergently-divergently oriented overlapping interference fringe systems allows to simultaneously measure tracer-particle velocities and corresponding positions within the laser-Doppler

measurement ellipsoid. The measurement concept was proposed by Czarske (2001) and subsequently further developed and improved (see e.g. Czarske et al., 2002; Büttner & Czarske, 2003, 2006; Bayer et al., 2008). More recently, the LDV-PS measurement technique was used to measure different flow scenarios, e. g. inside a hard disk drive model (Shirai et al., 2011, 2013) and in small-scale flow measurements in a fuel cell stack (Buerkle et al., 2020). A newly developed commercially available LDV-PS measurement system was used for measurements in the wake of a droplet (Burgmann et al., 2021) and in the oil flow in an open clutch test rig (Leister et al., 2022).

In the latter measurements a laminar rotational Couette-like flow with velocities of up to 1.64 m/s was captured in a small gap of 320 μm height. The parameters of the Fast Fourier Transform (FFT), i.e. sample rate and length, that was applied on the detected signal of tracer particles' scattered light were kept constant. The scattering of measured z -positions was observed to be wider at lower velocities and smaller at higher velocities. A procedure based on statistical averaging has been successfully applied due to the laminar behaviour of the observed flow. For turbulent flows, in contrast, the distinction of fluctuations and measurement uncertainty remains a challenging task for velocity-dependent measurement accuracies, which holds particularly true when superimposed to large velocity gradient. In this context, the present experimental study places particular emphasis on the interplay of the chosen acquisition parameters together with the velocity level, and the accuracy of the velocity and position estimation from an application perspective.

For general LDA systems the theoretical minimum achievable measurement accuracy is given by the Cramér-Rao lower bound (CRLB)

$$\sigma_f^2 = \frac{3f_s}{\pi^2 N(N^2 - 1)\text{SNR}} \quad (1)$$

where f_s is the sampling frequency, N the number of samples and SNR the signal-to-noise ratio (Ibrahim et al., 1991; Shinpaugh et al., 1992; Tropea, 1995; Tropea et al., 2007). Thus, while the minimum frequency measurement error increases with increasing sample frequency and decreasing sample number, no information is provided by the CRLB for the general behaviour of the measurement accuracy depending on the FFT parameters. However, it has been reported that the frequency error can be smaller when more samples are considered in the FFT evaluation of a burst signal (Rife & Boorstyn, 1974; Nakajima & Ikeda, 1990; Ibrahim et al., 1991; Gazengel et al., 2003).

Beyond the influence of signal processing parameters, additional uncertainty is expected from the finite size of the registered particles, such that the particle diameter has to be considered as an additional degree of freedom for the present study. To investigate influence and interplay of these factors on the resulting velocity- and position-estimation accuracy a characterization experiment is performed. Wires of varying diameter are distributed evenly along the perimeter of a circular frame, which is mounted at an existing clutch test rig (Leister et al., 2021) and operated at various (constant) angular velocities Ω . The wires accordingly serve as artificial tracers with known location, velocity and diameter for the comparative study of the different influential factors on the resulting measurement accuracy as will be elaborated below.

2. Measurement Technology

The LDV-PS builds upon the laser Doppler Velocimetry (LDV) measurement concept and comprises two laser-beam pairs $i = 1, 2$ with different wavelengths λ_i and overlapping interference fringe systems in the same plane. In contrast to a general LDV arrangement, the intersection points of the pairs are shifted from their respective beam-waist positions to the converging and diverging parts of the beams to purposely span two overlapping counter-oriented fan-shaped fringe patterns. Thus, the fringe distances d_i with $i = 1, 2$ of the interference patterns are a function of the z -position as illustrated in Figure 1. Since the registered Doppler-burst signals of a single particle – while simultaneously crossing both fringe patterns accordingly – rely on the location within the ellipsoid, the z -position can be determined with the quotient q of the received scattered light frequencies f_i of both fringe systems, i.e.

$$q(z) = \frac{f_2(z, u)}{f_1(z, u)} = \frac{u/d_2(z)}{u/d_1(z)} = \frac{d_1(z)}{d_2(z)} \quad (2)$$

as described by Czarske et al. (2002). The calibration function assigns a z -position value to a detected quotient q on basis of the fringe distances $d_i(z)$ as shown in Figure 2 for the considered pre-calibrated set-up.

Various post-processing routines have been suggested in literature to determine a velocity profile from the measured signals. Shirai et al. (2006) used the averaged position and velocity of 200 neighboring particle bursts, while Burgmann et al. (2021) averaged velocity values of bursts within the same $10 \mu\text{m}$ -range of detected z -positions. This comparison indicates that there is no standardized evaluation strategy of the acquired data. Considering the determination procedure of a passing tracer particle's velocity and position, it becomes furthermore clear that also the measurement accuracies of both quantities are linked to each other.

The standard deviations of a profile sensor have been derived theoretically for the z -position

$$\sigma_z \approx \sqrt{2} \left| \frac{\partial z}{\partial q} \right| \frac{\sigma_f}{f} \quad (3)$$

and velocity

$$\frac{\sigma_u}{u} \approx \sqrt{\frac{3}{2}} \frac{\sigma_f}{f} \quad (4)$$

by Czarske et al. (2002) assuming similar frequency levels and standard deviations in both fringe systems. It is consequently concluded, that the measurement accuracy depends on the accuracy at which the Doppler frequencies f_1 and f_2 are captured, the slope $\partial q / \partial z$ of the calibration curve and the accuracy of the calibration curve. The present study, therefore, focuses on the frequency estimation in the context of different acquisition concepts and wire diameters. A separate accuracy evaluation of z -position and velocity of measurement data is a nontrivial task, as an inaccurate estimation of the signal burst frequency can result in a deviation in both the z -location and/or the

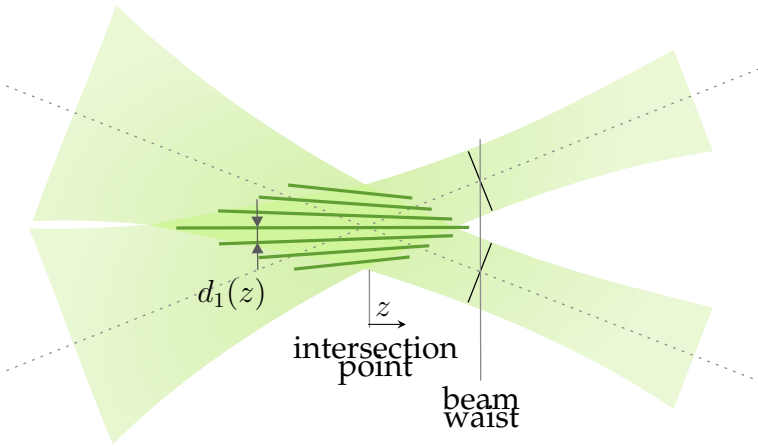


Figure 1. Convergent fringe pattern of one laser-beam pair with intersection point shifted from the beam waists.

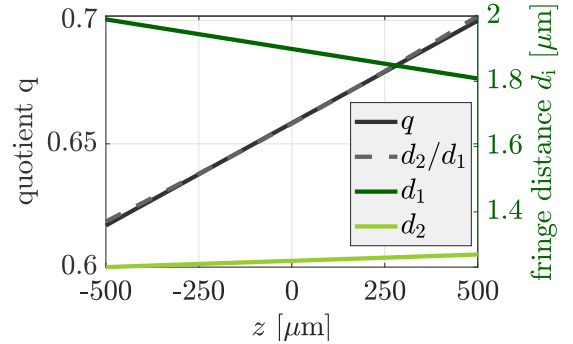


Figure 2. Linearized calibration curve $q(z)$ and associated fringe spacings $d_i(z)$.

velocity u . Accordingly, burst deviations from a resulting mean velocity profile are to be interpreted as combinations from either error source. The application of the above-mentioned spinning frame with wires of known diameter allows the supply of tracer signals at constant z -location and velocity, which in turn reduces the possible error sources during location and velocity estimation.

3. Experimental Procedure

Wires of $5\ \mu\text{m}$, $10\ \mu\text{m}$, $13\ \mu\text{m}$, $20\ \mu\text{m}$, $40\ \mu\text{m}$ and $80\ \mu\text{m}$ diameter have been glued radially oriented to a 3D-printed circular frame to ensure a constant circumferential velocity $u_\varphi = \Omega r$ of all wires for a given angular speed Ω ; see Figure 3. Tungsten hot wires were used for the study, as these are available with small diameters down to the order of magnitude of the size of seeding particles and with a good geometrical accuracy of diameter $\pm 10\%$. The frame was mounted on the rotating disk unit of a clutch test rig (see Leister et al., 2021, for rig details) and rotated by a precise *nanotec ST11018L8004* stepping motor at four different rotational velocities Ω . A light barrier sensor *WL100L-F2231* enabled the retro-active determination of the rotation angle to distinguish the measurement data of the individual wires and thus allocate the respective wire diameters. As the frame radius was large compared to the measurement volume, the trajectory of the wires through the measurement volume was approximately linear.

A commercial *ILA R&D 1D2C* LDV-PS comprised of two Nd:YAG lasers ($\lambda = 532\ \text{nm}$ and $\lambda = 552\ \text{nm}$) with a 5 MHz Bragg-shift was employed to measure the wire velocities and z -positions. The measurement system consists of an additional perpendicularly oriented laser component ($\lambda = 561\ \text{nm}$) for the determination of a second velocity component, which was not evaluated for the present experiments. The sensor was facing the wire frame and tilted towards the axis of rotation by 20° to avoid reflection issues on the wire frame surface underneath the wires. The set-up is shown in Figure 3.

In order to investigate the influence of different acquisition settings, the wires were detected at four

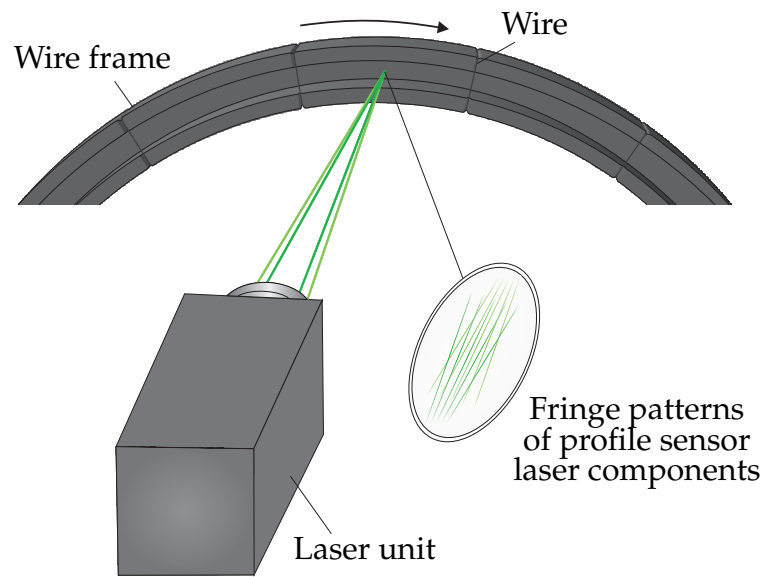


Figure 3. Measurement setup with LDV-PS in front of a rotating frame with radially applied wires.

rotational velocities in three different modes as illustrated in Figure 4 and parameter combinations as listed in Table 1. First, in case *a*, the acquisition rate and number of samples used for the FFT were held constant. This acquisition mode is especially advantageous, when the velocities of the investigated flow field are unknown. Furthermore, the measurement effort is comparatively small as all data can be acquired with the same set of parameters in one individual run. For case *b*, the sample rate was kept constant and the sample number was varied such as to adjust the acquisition-window width to the velocity-dependent length of the registered burst events. Lastly, in case *c*, the sample number per burst was kept constant and the sample rate was adjusted accordingly to record the constant number of samples across the same period length of a burst independent of the wire velocities. It is worth to mention that – in contrast to the simplicity of mode *a* – the acquisition settings have to be iteratively adjusted to the measured velocity for cases *b* and *c*, which makes flow measurements of velocity gradients more complex.

The measurement data of each mode and velocity was acquired in four consecutive measurements of 80 minutes, each followed by a break of 30 minutes to limit heating effects of the wires caused by the laser radiation, which might lead to elongation of the wires and thus a change of the dynamic behaviour. With this procedure at least 5000 bursts of each considered wire were detected in all acquisition modes and statistical convergence of the measurement data of the individual wires was accordingly confirmed. The statistical quantities of each acquisition parameter set were calculated by means of weighted averages and standard deviations of the four individual measurements.

Note that all wires were glued on the wire frame by hand, which implies possible differences in their positioning and tension influencing their dynamic behaviour when rotating. To reduce the influence of these effects, three wires of each diameter were mounted on the frame and simultaneously detected in the experiments. For the measurement evaluation only the wire showing the

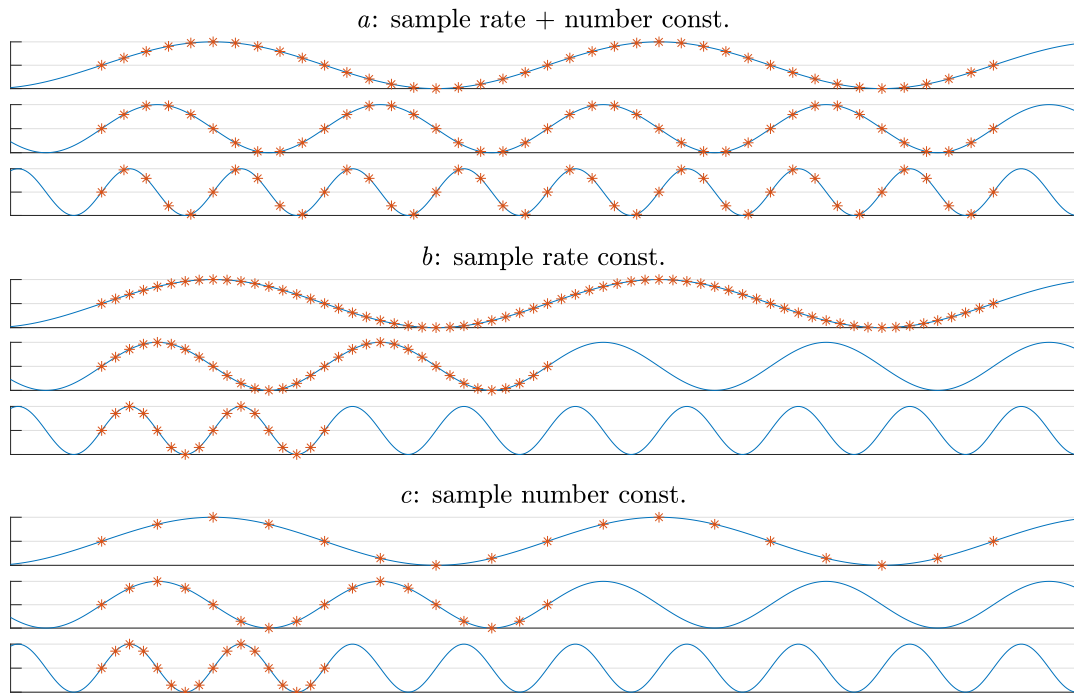


Figure 4. Illustration of the three different acquisition modes *a*, *b* and *c*.

Table 1. Acquisition settings of the individual measurements; reference case appears in **bold font**.

Rotation frequency Hz	Velocity m/s	Sample number	Sample rate MHz	Cases
1	0.55	2048	50	<i>a</i>
		4096	50	<i>b</i>
		2048	25	<i>c</i>
2	1.1	2048	50	<i>a, b, c</i>
4	2.2	2048	50	<i>a</i>
		1024	50	<i>b</i>
		2048	100	<i>c</i>
8	4.4	2048	50	<i>a</i>
		512	50	<i>b</i>
		2048	130*	<i>c</i>

* chosen value (below the desired $4 \times 50 = 200$ MHz) due to hardware limitation of the applied sensor

least dynamic behaviour was considered, as differences between individual wires of the same diameter can be related to the set-up and do not represent the character of seeding particles, which would be detected in flow measurements. Though, the positioning of the wires remains a possible source of measurement inaccuracy in these experiments, which has to be considered.

4. Results and Discussion

The conducted measurements comprise the three acquisition modes, four velocities and six wire diameters. For all bursts the frequencies and both fringe systems f_i with $i = 1, 2$, the accordingly calculated z position and the rotational velocity u were acquired.

Figure 5 shows the distributions of detected burst velocities and positions exemplary for the $5 \mu\text{m}$ and $80 \mu\text{m}$ diameter wires and all three acquisition modes. The z standard deviations σ_z are indicated by the black asterisks. As to be expected, σ_z decreases for thinner wires for all three acquisition cases. Figure 5 also shows that the scattering of the velocity values within the individual measurements is small. The relative standard deviation σ_u/u is in the range of 0.4% to 0.6% for all wires and cases with slightly increasing relative velocity standard deviations for larger wire diameters.

For acquisition case *a*, with constant sample rate and number for the FFT, the spatial uncertainty increases with decreasing velocities. This effect has also been observed in the clutch flow (Leister et al., 2022) and can be explained by the different representations of the burst signal by the evaluated samples. While the temporal window is equal, the period length decreases and the excluded margin of the registered bursts increases for lower velocities so that an accordingly smaller proportion of the burst signal is evaluated. The truncation of the burst signal goes along with a lack of information and is, therefore, expected to cause the observed measurement uncertainty to increase

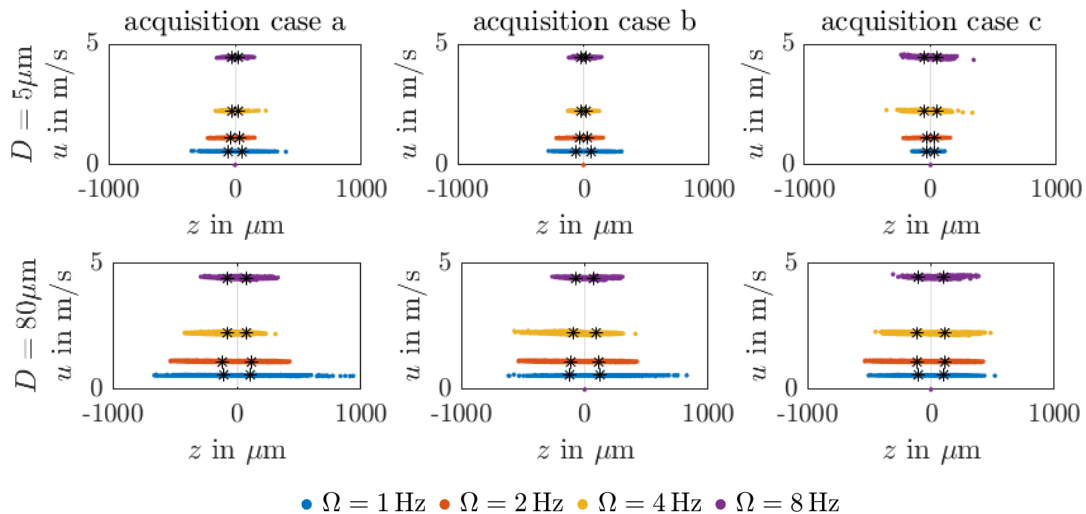


Figure 5. Distributions of detected wire velocities and corresponding positions for different velocity levels, wire diameters D and acquisition modes. The black asterisks mark the individual z -position standard deviations σ_z .

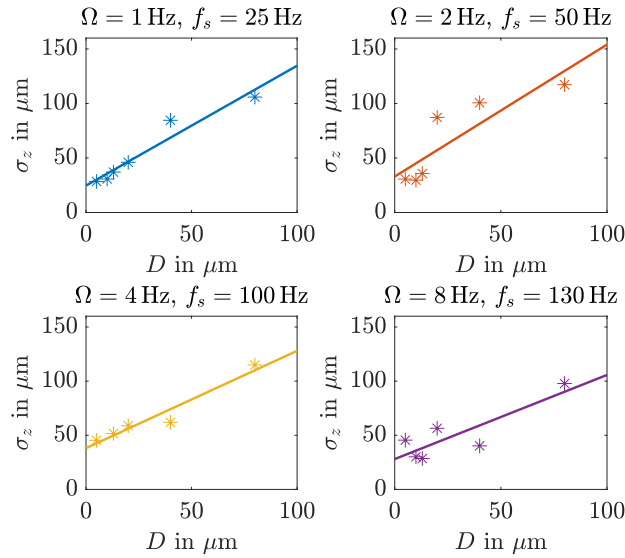


Figure 6. Individual values and fitted linear curve of z -position standard deviation over wire diameter D for the four individual velocity levels of acquisition mode c .

at low velocities. In mode c , the position-estimation uncertainty is observed to be independent from the considered velocity level. While the sample number was again kept constant, the sample rate was adjusted so that the period resolution and period length of a burst signal are equal for all considered wire velocities. This analogous description of the burst signals is likely to cause a constant accuracy. The relative signal length is also constant for all velocities in case b , while the period resolution is higher for smaller velocities (cp. Figure 5). Similar effects can be observed as in case a , which again implies an increasing uncertainty for lower velocity levels.

Figure 6 shows the z -position standard deviations σ_z over the wire diameter D for the individual wire diameters at the four different wire velocities and corresponding acquisition settings of mode c . A linear function for $\sigma_z(D)$ was calculated by means of a least-square fits for each individual measurement. The linear curves $\sigma_z(D)$ for all measurements are shown in Figure 7 separated by their acquisition cases. For cases a and b , the curves are sorted according to the wire velocity, as the standard deviation increases for decreasing velocities as shown earlier. For acquisition case c , the curves collapse and their arrangement to each other is not connected to the represented velocity. The slope dz/dD of the curves varied in the range from 0.67 to 1.21 with an average slope of 0.91 close to 1 for all three acquisition cases. Thus, the hypotheses can be stated that the z -position standard deviation increases by the same value as the wire or particle diameter. Furthermore, σ_z might be limited to the particle diameter as a minimum, since light is scattered at the particle surface when passing the measurement volume.

The absolute level of observed standard deviations is additionally influenced by sources of uncertainty related to the experimental set-up. These include the wire diameter uncertainty, the hand-mounting process of the wires, vibrations of the test rig, thermo-mechanical effects on the wires caused by the laser radiation and possibly velocity dependent dynamic behaviour of the

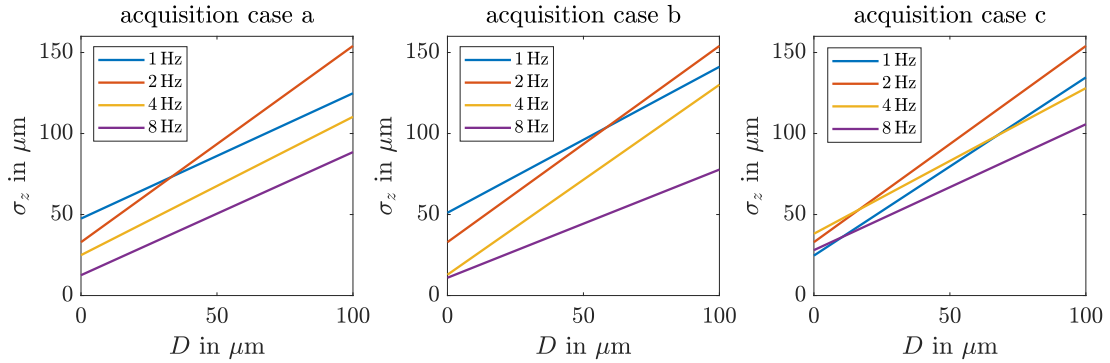


Figure 7. Fitted linear curves for z -position standard deviation over wire diameter D for all four velocity levels of acquisition modes a , b and c .

wires. Most of these factors can not be determined quantitatively for the conducted experiments. However, a triangulation sensor was employed to capture vibrations of the test rig. Those measurements were carried out separately without the LDV-PS system being mounted to the test rig, which might have additionally influenced the dynamical behaviour. At the radius at which the wires velocities and positions were measured, the vibration-caused z -position fluctuations were found to be $9.8 \mu\text{m}$ at 0.5 Hz , $12.7 \mu\text{m}$ at 1 Hz and $24.1 \mu\text{m}$ at 2.0 Hz . Subtracting these errors from the z -position standard deviations would correspond to vertical shifting of the $\sigma_z(D)$ -curves in Figure 7 accordingly.

In regard of the measurement uncertainty estimations given in Equations (3) and (4), the mentioned factors influence the frequency standard deviation σ_f together with measurement accuracy effects. The latter depend on the signal processing procedure for the frequency estimation of a burst signal, i.e. the effect of the different acquisition cases. Additionally, σ_z depends on the quotient function slope $\partial z/\partial q$ and the quotient function accuracy (Czarske et al., 2002). For the used LDV-PS measurement system, the quotient function is approximated by a linear function as illustrated in Figure 2, which causes an increasing measurement error with increasing distance from the measurement volume center at $z = 0$. The slope $\partial z/\partial q$ of the used measurement system is $12\,041 \mu\text{m}$, whereas a slope of $7\,143 \mu\text{m}$ was reported for a different LDV-PS set-up by Shirai et al. (2006), which approximately halves the calculated z -position standard deviation. This difference in the slope of the quotient function occurs due to a larger focal length of the commercial LDV-PS system. With the frequency values $f_i, i = 1, 2$ captured in the measurements the theoretical values for σ_z and σ_u/u were approximated using Equations (3) and (4), and the results are in good correspondence with the actually observed values of the z and u standard deviations.

5. Conclusions and Outlook

In the present study, different acquisition settings have been systematically applied to a commercial LDV-PS system in order to understand their influence on the measurement system's position and velocity measurement accuracies. For acquisition mode a , with constant FFT parameters, the

z -position standard deviation was found to increase with decreasing velocity levels. This effect was successfully avoided in acquisition mode c , where the sampling frequency was adjusted according to the velocity level to achieve an equal period resolution and period length. Thus, the acquisition settings have been shown to strongly influence the obtained measurement accuracy. These findings offer the users of commercial systems the possibility to choose more targeted FFT parameters to optimize the signal processing in future measurements. Consequently, the LDV-PS measurement accuracy can be adjusted by appropriately chosen boundary conditions. However, for flows with high velocity gradients the acquisition settings need to be adjusted to the local flow velocities individually to avoid decreasing measurement accuracy at lower flow velocities. This approach requires pre-knowledge about the present flow structures and might increase the measurement duration and evaluation effort.

The relative velocity standard deviation was found to be rather small as it varied in the range of 0.4% to 0.6% for all FFT-parameter and wire-diameter combinations. Accordingly and in accordance with earlier measurements in the clutch gap (Leister et al., 2022), for very slow flow velocities in correspondence with a large z -position standard deviation, it seems advantageous to average measured position values within velocity slots instead of averaging velocity values within position slots during data post-processing.

Furthermore, the conducted experiments reveal the effects of different sizes of scattering objects, represented by wires of varying diameters, on the position measurement accuracy of a LDV-PS measurement system. For increasing diameters, the position standard deviation σ_z has been found to increase by almost the same rate, with an average gradient of $\partial\sigma_z/\partial d = 0.91$.

In laminar flow scenarios, measurements with a commercial LDV-PS system have been conducted successfully by means of a statistical evaluation of averaged velocity profiles as discussed by Leister et al. (2022). The present parametric study further revealed the cause-effect relations between the observed measurement uncertainty and the underlying choice of experimental set-up and FFT-processing parameters.

However, measurements in wall-bounded shear flows with high velocity gradients remain a challenging task, which will be approached in future investigations. For measurements in turbulent flows – and inside the viscous sublayer in particular – mean velocity profiles should be studied in the first place. Subsequently, for the acquisition of Reynolds-Stresses, fluctuations and measurement error need to be distinguished. Therefore, comparisons with reference measurement and/or DNS data can verify the experimental procedure and new evaluation routines.

Nomenclature

σ_f	frequency standard deviation [Hz]
f_s	sampling frequency [Hz]
N	number of samples

$\lambda_i, i = 1, 2$	wavelength [m]
z	position coordinate [m]
u	velocity [m/s]
$d_i, i = 1, 2$	interference fringe distance [m]
$f_i, i = 1, 2$	frequency [Hz]
q	quotient function
σ_z	position standard deviation [m]
σ_u	velocity standard deviation [m/s]
Ω	angular speed [Hz]
r	radius [m]
D	wire diameter [d]

References

- Bayer, C., Shirai, K., Büttner, L., & Czarske, J. (2008). Measurement of acceleration and multiple velocity components using a laser doppler velocity profile sensor. *Measurement Science and Technology*, 19(5), 055401.
- Buerkle, F., Moyon, F., Feierabend, L., Wartmann, J., Heinzl, A., Czarske, J., & Büttner, L. (2020). Investigation and equalisation of the flow distribution in a fuel cell stack. *Journal of Power Sources*, 448, 227546.
- Burgmann, S., Dues, M., Barwari, B., Steinbock, J., Büttner, L., Czarske, J., & Janoske, U. (2021). Flow measurements in the wake of an adhering and oscillating droplet using laser-doppler velocity profile sensor. *Experiments in Fluids*, 62(3), 1–16.
- Büttner, L., & Czarske, J. (2003). Spatial resolving laser doppler velocity profile sensor using slightly tilted fringe systems and phase evaluation. *Measurement Science and Technology*, 14(12), 2111.
- Büttner, L., & Czarske, J. (2006). Determination of the axial velocity component by a laser-doppler velocity profile sensor. *JOSA A*, 23(2), 444–454.
- Czarske, J. (2001). Laser doppler velocity profile sensor using a chromatic coding. *Measurement Science and Technology*, 12(1), 52.
- Czarske, J., Büttner, L., Razik, T., & Müller, H. (2002). Boundary layer velocity measurements by a laser doppler profile sensor with micrometre spatial resolution. *Measurement Science and Technology*, 13(12), 1979.
- Gazengel, B., Poggi, S., & Valière, J.-C. (2003). Evaluation of the performance of two acquisition and signal processing systems for measuring acoustic particle velocities in air by means of laser doppler velocimetry. *Measurement Science and technology*, 14(12), 2047.

- Ibrahim, K., Wertheimer, G., & Bachalo, W. D. (1991). Signal processing considerations for low signal to noise ratio laser doppler and phase doppler signals. In *Proc. 4th intl. conf. on laser anemometry, cleveland, oh.*
- Leister, R., Fuchs, T., Mattern, P., & Kriegseis, J. (2021). Flow-structure identification in a radially grooved open wet clutch by means of defocusing particle tracking velocimetry. *Experiments in Fluids*, 62(2), 1–14.
- Leister, R., Pasch, S., & Kriegseis, J. (2022). On the applicability of phase-resolved ldv profile-sensors for open wet clutch flow scenarios. *Experiments in Fluids*, revised manuscript under review.
- Nakajima, T., & Ikeda, Y. (1990). Theoretical evaluation of burst digital correlation method for ldv signal processing. *Measurement Science and Technology*, 1(8), 767.
- Rife, D., & Boorstyn, R. (1974). Single tone parameter estimation from discrete-time observations. *IEEE Transactions on information theory*, 20(5), 591–598.
- Shinpaugh, K., Simpson, R., Wicks, A., Ha, S., & Fleming, J. (1992). Signal-processing techniques for low signal-to-noise ratio laser doppler velocimetry signals. *Experiments in Fluids*, 12(4), 319–328.
- Shirai, K., Büttner, L., Obi, S., & Czarske, J. (2013). An experimental study on the flow behavior near the read-and-write arm in a hard disk drive model with a shroud opening. *Microsystem technologies*, 19(9), 1519–1527.
- Shirai, K., Pfister, T., Büttner, L., Czarske, J., Müller, H., Becker, S., ... Durst, F. (2006). Highly spatially resolved velocity measurements of a turbulent channel flow by a fiber-optic heterodyne laser-doppler velocity-profile sensor. *Experiments in fluids*, 40(3), 473–481.
- Shirai, K., Yaguchi, Y., Büttner, L., Czarske, J., & Obi, S. (2011). Highly spatially resolving laser doppler velocity measurements of the tip clearance flow inside a hard disk drive model. *Experiments in fluids*, 50(3), 573–586.
- Tropea, C. (1995). Laser doppler anemometry: recent developments and future challenges. *Measurement Science and Technology*, 6(6), 605.
- Tropea, C., Yarin, A. L., & Foss, J. F. (2007). *Springer handbook of experimental fluid mechanics* (Vol. 1). Springer.